

Scattering of magnons at graphene quantum-Hall-magnet junctions

Nemin Wei, Chunli Huang, and Allan H. MacDonald

Department of Physics, The University of Texas at Austin, Austin, Texas 78712, USA

Motivated by recent non-local transport studies of quantum-Hall-magnet (QHM) states formed in monolayer graphene's $N = 0$ Landau level, we study the scattering of QHM magnons by gate-controlled junctions between states with different integer filling factors ν . For the $\nu = 1|-1|1$ geometry we find magnons are weakly scattered by electric potential variation in the junction region, and that the scattering is chiral when the junction lacks a mirror symmetry. For the $\nu = 1|0|1$ geometry, we find that kinematic constraints completely block magnon transmission if the incident angle exceeds a critical value. Our results explain the suppressed non-local-voltage signals observed in the $\nu = 1|0|1$ case. We use our theory to propose that valley-waves generated at $\nu = -1|1$ junctions and magnons can be used in combination to probe the spin/valley flavor structure of QHM states at integer and fractional filling factors.

Introduction– The recent discovery of magnetic order in two-dimensional materials [1–5] has suggested new strategies to build ultra-compact spintronic devices that utilize magnons as weakly dissipative information carriers [6–8]. Ordered states, referred to generically as quantum Hall magnets (QHMs), occur in graphene in a strong magnetic field and break spin and valley symmetries [9–25]. Because of their electronic simplicity and gate tunability, and also because the technology needed to prepare extremely clean and well characterized monolayer graphene samples is well established [26–29], graphene QHMs are an excellent system in which to demonstrate two-dimensional spintronic and magnonic device concepts.

When a strong magnetic field is applied perpendicular to a 2D graphene sheet, the π -orbitals of the carbon atoms form Landau levels with approximate four-fold isospin degeneracy. The isospin degeneracy combines a two-fold valley pseudospin with the electron spin degree of freedom. In a partially filled Landau level, Coulomb interactions often break the Hamiltonian's $SU(4)$ isospin symmetry and give rise to a rich family of correlated insulating states. At an integer filling factor, the ground-state is a single Slater determinant and can be therefore described by Hartree-Fock mean-field theory [24, 30, 31]. At filling factor $\nu = \pm 1$, *i.e.* at three-quarter and one quarter-filling of the $N = 0$ Landau level quartet, the ground-state is analogous to the QHM states found in two-dimensional electron gases in semiconductor quantum wells and consists of fully spin and valley polarized electrons ($\nu = -1$) or holes ($\nu = 1$) [32]. In contrast, the ground state at filling factor $\nu = 0$ (half-filling of the $N = 0$ Landau level) is more complicated. As pointed out by Kharitonov [24], the $\nu = 0$ phase-diagram contains a ferromagnet (F), a canted antiferromagnet (CAF), a Kekulé distortion state, and a charge density wave. The competition between these states is influenced by weak lattice-scale Coulomb interactions that break $SU(4)$ symmetry, sample-dependent substrate-induced sublattice polarization potentials [33–35], dielectric screening [36] and in-plane magnetic fields. The systematic [13] dependence on

in-plane magnetic field of an edge-state metal-insulator transition strongly suggests that the $\nu = 0$ ground state is a canted antiferromagnet (CAF) in which opposite valleys have different spin polarizations. The ordered states at $\nu = 0, \pm 1$ support low-energy collective excitations [16–18] that are analogous to magnon modes in a conventional magnetic systems, and which we will refer to as QH magnons.

Recent experiments [37–39] have studied the transmission of QH magnons through junctions between distinct QHM states. In Ref. [38, 39], $\nu = 1$ QH magnons are generated electrically by driving magnon-mediated transitions between conducting edge states with different spin-orientations. The change in conduction spin is transferred to a magnon that can be propagated through the two-dimensional bulk. (See Ref. [40] for a theoretical model of the magnon generation process.) Magnons are then guided toward $1|\nu_m|1$ QHM junctions, where ν_m is a (gate-tunable) filling fraction of interest sandwiched between $\nu = 1$ regions. Any magnons transmitted through the junction generate non-local electrical signals on the opposite side of the device via the reciprocal of the magnon generation process. Measured non-local voltages suggest that the $1|-1|1$ junction is nearly transparent for magnons, since the non-local voltage signal is not greatly reduced by its presence. In contrast, the non-local voltage signal is greatly suppressed by $\nu = 1|0|1$ junctions. This finding requires an explanation since the $\nu_m = 0$ canted antiferromagnet also supports magnons [41–43].

In this Letter, we use microscopic theory to calculate magnon transmission through $1|\nu_m|1$ QHM junctions. For $\nu_m = -1$ we find that although the magnon modes are identical in all regions, the electrostatic inhomogeneity of the junction partially reflects magnons. The $\nu_m = 0$ CAF state has two magnon branches that, except at very small momenta, have higher energies than $\nu = 1$ magnons. We find that this energy mismatch leads to perfect reflection above a critical angle of incidence Θ_c , explaining the difference in non-local electrical signals.

Time Dependent Hartree-Fock Theory– We formulate the problem of collective-mode transmission by studying

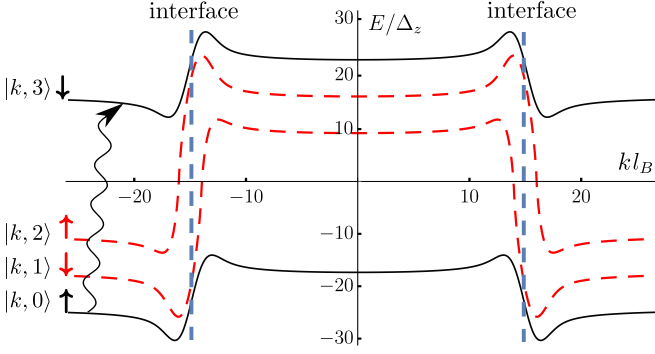


Figure 1. Self-consistent Hartree-Fock bandstructure of a $1|-1|1$ junction in which the sense of valley polarization is opposite in the $\nu = 1$ and $\nu = -1$ regions. The uniform $\nu = 1$ and $\nu = -1$ states have majority (\uparrow) spin occupation selected by the weak Zeeman coupling and, for unaligned hBN encapsulation, spontaneously chosen valley polarization. The black solid lines show valley K quasiparticle energies *v.s.* guiding center, and the red dashed lines show the valley K' orbitals that cross the Fermi level ($E_F = 0$) at $\nu = 1|-1$ junctions. The curly line represents the bands involve in particle-hole transition of a $\nu = \pm 1$ magnon.

the dynamics of the $N = 0$ Landau level single-particle density-matrix

$$i\partial_t \hat{P}(t) = [\hat{H}, \hat{P}(t)], \quad (1)$$

where \hat{H} is the mean-field Hamiltonian determined self-consistently at each instant in time:

$$\hat{H}_{k+q_y, k} = \hat{H}_k^0 \delta_{q_y, 0} + \hat{\Sigma}_{k+q_y, k}^H + \hat{\Sigma}_{k+q_y, k}^F, \quad (2a)$$

$$\hat{H}_k^0 = \frac{\Delta_z}{2} s^z + \frac{\Delta_v}{2} \tau^z + E_b(k), \quad (2b)$$

$$\hat{\Sigma}_{k+q_y, k}^H = \sum_{\alpha=0}^3 \sum_{k'} V_{\alpha}(k - k', q_y) \text{tr}(\tau^{\alpha} \hat{P}_{k'+q_y, k'}^{\alpha}) \tau^{\alpha}, \quad (2c)$$

$$\hat{\Sigma}_{k+q_y, k}^F = - \sum_{\alpha=0}^3 \sum_{k'} V_{\alpha}(q_y, k - k') \tau^{\alpha} \hat{P}_{k'+q_y, k'}^{\alpha} \tau^{\alpha}. \quad (2d)$$

The single-particle Hamiltonian \hat{H}_k^0 , specified in Eq. (2b), includes Zeeman energy ($\Delta_z = g\mu_B|B|$), valley-polarization energy (Δ_v) and background electrostatic (E_b) energy contributions. Δ_v is induced by adjacent hBN layers if aligned and E_b controls the spatial variation of filling fraction. Here \mathbf{s} ($\boldsymbol{\tau}$) are Pauli matrices in spin (valley) space and the wavevectors k are Landau gauge momenta in the direction along the junction line. The electrostatic background potential E_b is k dependent because Landau gauge eigenstates are localized along guiding center lines with x -coordinate $X = kl_B^2$, where l_B is the magnetic length. In Eqs. (2c)–(2d), the $\alpha = 0$ and $\alpha = 1, 2, 3$ self-energy terms account respectively for the SU(4) invariant long-range Coulomb interaction and the short-range valley-dependent interactions.[44] The time-independent self-consistent solutions of Eq. (1) preserves

Table I. Properties of the magnon mode ω_s of the $\nu = 1$ F state and the two magnon modes $\omega_{1,2}$ of the $\nu = 0$ CAF state. The CAF modes are linear-combinations of spin-flips in the K and K' valleys and capture the quantum dynamics of the Néel \mathbf{n} and spin-polarization \mathbf{m} vectors. $\phi_{mn}(\mathbf{q}) \equiv \sum_{\mathbf{k}} e^{iq_x kl_B^2} \psi_{kmn}(q_y)$. [44]

	$(\phi_{30}, \phi_{21}, \phi_{12}, \phi_{03})$	Gap	Description
ω_s	$(1, 0, 0, 0)$	Δ_z	spin precession within a valley
ω_1	$(u_{1\mathbf{q}}, u_{1\mathbf{q}}, v_{1\mathbf{q}}, v_{1\mathbf{q}})$	0	in-plane($\perp \mathbf{B}$) oscillation of \mathbf{n}
ω_2	$(u_{2\mathbf{q}}, -u_{2\mathbf{q}}, v_{2\mathbf{q}}, -v_{2\mathbf{q}})$	Δ_z	precession of \mathbf{m} about \mathbf{B} field

translational symmetry along the junction line and is therefore diagonal in k [45]:

$$\hat{P}_{k+q_y, k}^0 = \delta_{q_y, 0} \sum_{m=0}^3 f_{m, k} |k, m\rangle \langle k, m|, \quad (3)$$

where $|k, m\rangle$ is the m -th mean-field band ordered energetically from 0 to 3 and $f_{m, k}$ is its occupation number. We plot the quasiparticle bandstructure of a $\nu = 1|-1|1$ junction in Fig. 1 for future reference. To describe small amplitude dynamics, we expand $\hat{P}(t) = \hat{P}^0 + \delta\hat{P}(t)$ and use the compact notation

$$\psi_{kmn}(q_y) \equiv \langle k + q_y, m | \delta\hat{P} | k, n \rangle, \quad (4)$$

to denote particle-hole transition amplitudes with momentum q_y . When linearized in $\delta\hat{P}$, Eq. (1) implies that

$$\omega \psi_{kmn}(q_y, \omega) = \sum_{k' m' n'} \mathbb{K}_{kmn}^{k' m' n'}(q_y) \psi_{k' m' n'}(q_y, \omega), \quad (5)$$

where ω is the collective mode frequency and $\mathbb{K}_{kmn}^{k' m' n'}$ is known as the RPA (random-phase approximation [41–43, 46, 47]) kernel that acts as a superoperator on the collective mode ψ [44].

Magnon Scattering– The magnon scattering problem is complicated by the strong non-locality of the RPA kernel $\mathbb{K}_{kmn}^{k' m' n'}(q_y)$. In the absence of a junction $\mathbb{K}_{kmn}^{k' m' n'}(q_y)$ is invariant under simultaneous translation of guiding centers kl_B^2 and $k'l_B^2$, allowing Eq. 5 to be solved by Fourier transformation to obtain bulk modes labelled by two-dimensional wavevectors $\mathbf{q} = (q_x, q_y)$ with energies $\omega_i(\mathbf{q})$. Some key properties of the bulk collective modes are briefly summarized in Table. I. Since q_y remains a good quantum number in the presence of a $1|\nu_m|1$ junction, we are left with a q_y -dependent one-dimensional scattering problem with the $\nu = 1$ bulk modes as asymptotic states. We therefore apply the scattering boundary conditions:

$$\begin{aligned} \psi_{k30}(q_y, \omega) &= \begin{cases} e^{iq_x kl_B^2} + r(q_y, \omega) e^{-iq_x kl_B^2}, & k \rightarrow -\infty \\ t(q_y, \omega) e^{iq_x kl_B^2}, & k \rightarrow \infty \end{cases} \\ \psi_{kmn}(q_y, \omega) &= 0, \quad k \rightarrow \pm\infty \text{ and } m, n \neq (3, 0). \end{aligned} \quad (6)$$

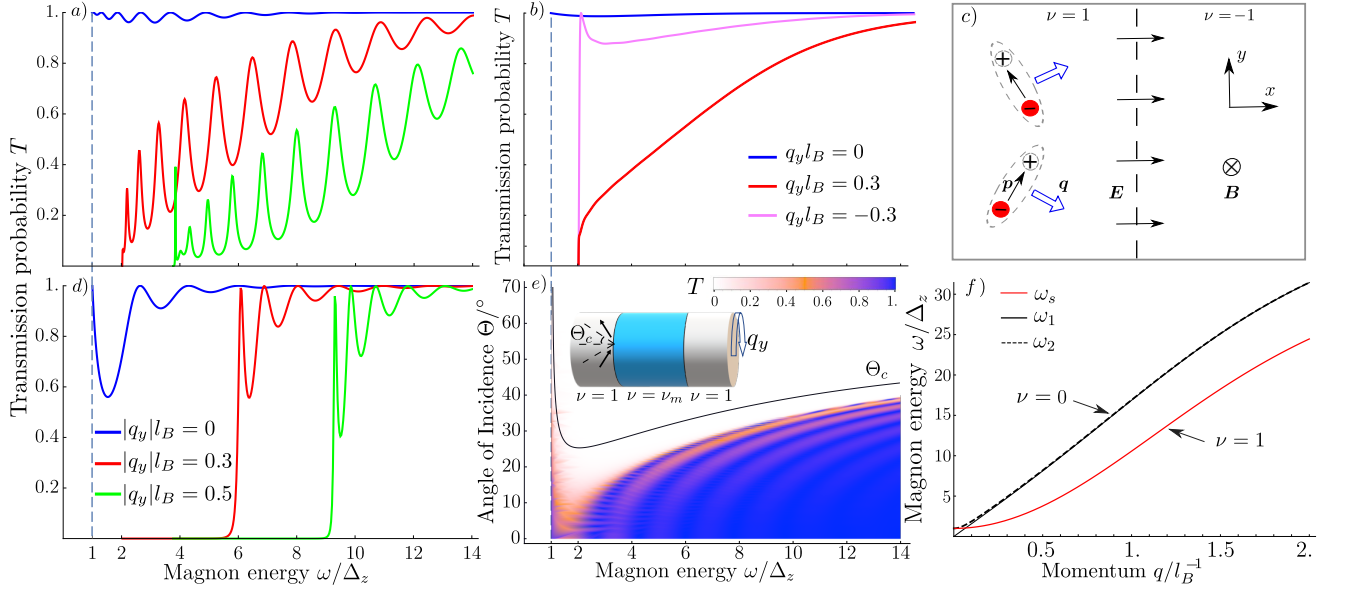


Figure 2. Magnon transmission probabilities $T(q_y, \omega)$ v.s. ω for $\nu = 1| - 1|1$ (a), $\nu = 1| - 1$ (b) and $\nu = 1|0|1$ (d) QHM junctions[44]. c) Schematic particle-hole pairs in $\nu = 1| - 1$ junctions. The interfacial electric field \mathbf{E} points from $\nu = 1$ to $\nu = -1$. Negative (positive) signs represents electrons (holes). The dipole moment \mathbf{p} of electron-hole pairs is perpendicular to both the magnetic field \mathbf{B} and the center-of-mass momentum \mathbf{q} . e) Color plot of the magnon transmission probability through a $\nu = 1|0|1$ junction vs. energy and angle of incidence. f) Magnon dispersions in uniform $\nu = \pm 1$ F states (ω_s) and in $\nu = 0$ ($\omega_{1,2}$) CAF states. These results are generated with experimentally determined Coulomb interaction strength at $B = 8T$ in a geometry with width $L_y = 80\pi l_B$ and the length of ν_m region is $30l_B$.

The asymptotic states are pure (ψ_{k30}) $\nu = 1$ magnons that are gapped by the Zeeman energy [38, 39]. In Eq. (6) q_x is determined by solving $\omega_s(\mathbf{q}) = \omega$. We solve for the scattering states and the q_y -dependent reflection $r(q_y, \omega)$ and transmission $t(q_y, \omega)$ coefficients by discretizing k , applying Eq. 5 at $j = 1, \dots, N$ points in a scattering region centered on the junction, and substituting the asymptotic expressions for $\psi_{k'm'n'}(q_y, \omega)$ at $j = 1$, $j = N$, and outside the junction. Only the $m, n = (3, 0)$ RPA equation is applied at $j = 1$ and $j = N$, which are assumed to be in the asymptotic region. This procedure yields a set of inhomogeneous linear equations [44] that we have converged with respect to guiding center mesh density to obtain the results discussed below.

Magnon Transmission Results— Our results for the magnon transmission probabilities $T(q_y, \omega) = |t(q_y, \omega)|^2$ of $1|\nu_m|1$ QHM junctions with $\nu_m = -1$ and $\nu_m = 0$ are shown in Figs. 2a) and d) respectively. Both junctions have a threshold energy ω_{tr} , below which there is no transmission, $T(q_y, \omega < \omega_{tr}) = 0$. For a $1| - 1|1$ junction, the bulk $\nu = \pm 1$ regions have identical magnon dispersions, so the threshold energy is simply the bulk magnon energy at normal incidence: $\omega_{tr} = \omega_s(0, q_y)$. For $\omega > \omega_{tr}$, we find magnon transmission decreases with increasing q_y . The reduction is due to a peculiar property of collective mode excitations in quantum Hall systems, namely that the centre-of-mass momentum \mathbf{q} of a particle-hole excitation is related to its electric-dipole

moment \mathbf{p} by [48–50], $\mathbf{p} = |e|l_B^2 \hat{\mathbf{z}} \times \mathbf{q}$, as illustrated in Fig. 2c). Magnons with larger q_y scatter more strongly off the electric fields $E\hat{x}$ present in the junction region. When we examine the $1| - 1$ and $-1|1$ junctions separately, we find that magnons with opposite signs of q_y have different transmission probabilities, as shown in Fig. 2b). This behavior is expected since the $1| - 1$ junction acts like a repulsive scatterer when the dipole moment has an \hat{x} projection opposite to the the junction electric field, and like an attractive scatterer when the \hat{x} projection has a dipole moment that is aligned with the junction electric field. The total transmission through the $1| - 1|1$ junction plotted in Fig. 2a) and d) has $q_y \rightarrow -q_y$ symmetry because the studied model has mirror symmetry about the $y - z$ plane at the center of the $\nu = \nu_m$ region. We have verified that the junction scattering becomes chiral when this symmetry is absent.

The threshold energy ω_{tr} in Fig. 2d ($1|0|1$ junction) appears to be significantly larger than in Fig. 2a ($1| - 1|1$ junction). The suppressed magnon transmission is due to a mismatch between CAF and F collective mode dispersions. As shown in Fig. 2f), the bulk collective modes of $\nu = 0$ CAFs disperse more strongly than those of $\nu = 1$ Fs, so that $\omega_{1,2}$ has higher energy than ω_s , except at very small momenta where ω_1 is gapless while ω_2 and ω_s are gapped. To transmit a $\nu = 1$ magnon with energy $\omega = \omega_s$ and parallel momentum q_y through $1|0|1$ junction, the con-

servation of energy and parallel momentum requires that

$$\omega_s(q_x^L, q_y) = \omega_1(q_x^R, q_y), \quad (7)$$

where $q_x^{L/R} \geq 0$ are the asymptotic normal momenta on the left (L) and right (R) sides of the 1|0 junction. We identify the threshold energy as $\omega_1(0, q_y)$, the value of ω for which $q_x^R \rightarrow 0$. Since $\omega_1(0, q_y) > \omega_s(0, q_y)$ we conclude that the 1|0|1 junction has a higher threshold energy than 1|−1|1 junction. Once the incoming magnon energy exceeds $\omega_{tr}(q_y)$, as illustrated in Fig. 2d, T rapidly approaches 1. This property can be understood by noting the valley polarization of superpositions of ω_1 and ω_2 modes vary on the long length scale $\lambda_0 = 2\pi/(q_{x1}^R - q_{x2}^R)$, where q_{x1}^R and q_{x2}^R are the nearly identical local x wavevectors of the nearly degenerate (Fig. 2f) $\omega_{1,2}$ modes. A $\nu = 0$ magnon can therefore maintain the valley polarization of the $\nu = 1$ magnon across the junction, provided that the ν_m region is shorter than λ_0 . Our results for 1|0|1 junction magnon transmission are summarized in Fig. 2e), in which the transmission probability is plotted as a function of energy and angle of incidence $\Theta = \arctan(q_y/q_x^L)$. The black curve shows the critical incident angle Θ_c , obtained by solving Eq. (7) with $q_x^R = 0$. For higher angles of incidence, momentum and energy conservation imply that the magnons are evanescent waves in the $\nu = 0$ region.

The transmission probabilities in Fig. 2 exhibit Fabry-Pérot oscillations generated by the repeated scattering at the two interfaces. The interference pattern will be smeared out in observables that average magnons over angles of incidence. Assuming that all angles of incidence are equally likely, we define an average magnon transmission probability

$$\bar{T}(\omega) \equiv \frac{1}{\pi} \int_{-\pi/2}^{\pi/2} d\theta T(q_y(\theta, \omega), \omega). \quad (8)$$

As shown in Fig. 3a), the average transmission \bar{T} through a 1|0|1 junction is noticeably smaller than the transmission through a 1|−1|1 junction at low energies but becomes comparable to a 1|−1|1 junction at high energy. In our calculation of 1|0|1 junction we assumed perfect screening of induced Hartree potentials in the junction region by nearby gates [45]. Since the inhomogeneity of the electrostatic potential is a source of magnon-reflection, the transmission through a 1|0|1 junction would be even lower if we accounted for imperfect screening.

Discussion:— We now use our findings to interpret the experimental results in Ref. [38] and to propose related studies that might be informative. Magnons can be generated electrically by bringing edge channels with opposite spins and different chemical potentials together at a hot spot, opening a path for magnon-generation mediated edge-channel spin flips. The energies of magnons generated in this way must be smaller than the electrical bias voltage. We assume [40] that the steady state

established by electrically injected magnons [38], can be characterized by a magnon distribution with a well defined local chemical potentials. Non-local voltages generated by the reciprocal of the injection process measure local magnon chemical potentials. Non-local voltages measured at points that are separated from the injection point by a 1|0|1 junction, are small even when the electrical bias voltages is ~ 5 times [38] larger than Δ_z . This behavior is explained by the larger energies of magnons in $\nu = 0$ regions compared to $\nu = 1$ regions, as explained above. The slow increase in average transmission probability \bar{T} with magnon energy we find is also in agreement with experimental trends. We do find that a peak in \bar{T} (c.f. Fig. 3a) in a narrow window of energy ($1 < \omega/\Delta_z < 1.2$) just above Δ_z where the $\nu = 0$ and $\nu = 1$ magnon energies are more similar that is not detected experimentally, presumably because magnon generation in this energy window is not sufficient to produce an observable signal.

The experimental non-local signals of 1|1|1 and 1|−1|1 junctions are similar for bias voltages $\lesssim 5\Delta_z$, and much larger than the voltages measured in the 1|0|1 case. In our theory this property is due to the fact that $\nu = 1$ and $\nu = -1$ magnon modes have identical dispersions and therefore no kinematic transmission constraints. Our theory does predict finite reflection at 1|−1|1 junctions that is absent in the translationally invariant 1|1|1 case, but this will not be observable if unintended scattering from disorder or the split gate junctions dominates magnon scattering. Indeed, as we have emphasized, our calculation has identified the electrical dipole moments of QH magnons as a mechanism for magnon scattering off variations in electrical potential. Other extrinsic mechanisms such as spin-dependent disorder [51–53] near the sample edges can also suppress magnon transmission but are unlikely to play a dominant role in high quality devices used in Refs. [38, 39]

In closing we propose an experimental protocol illustrated schematically in Fig. 3b) to electrically detect valley ordering, e.g. Kekulé distortion, by measuring valley-wave transmissions. To inject valley-waves, we replace the 2|1 interface [38] used for magnon-injection with a −1|1 interface. As shown in Fig. 3c), when the −1|1 interface receives finite valley polarization potential from the aligned hBN, the mean-field bandstructure hosts two edge states with opposite valley polarization and nearly parallel spins whose chemical potentials can be independently controlled via the contacting geometry illustrated in Fig. 3b). The bias voltage opens up a path for valley-wave generation scattering between edge channels. In order to increase valley-wave emission probability, the edge states can be brought into close proximity via a quantum point contact. We expect the emitted valley-waves to be transmitted through ground states that support valley-wave excitations. Measuring non-local voltages provides a new method to determine the isospin structure of quan-

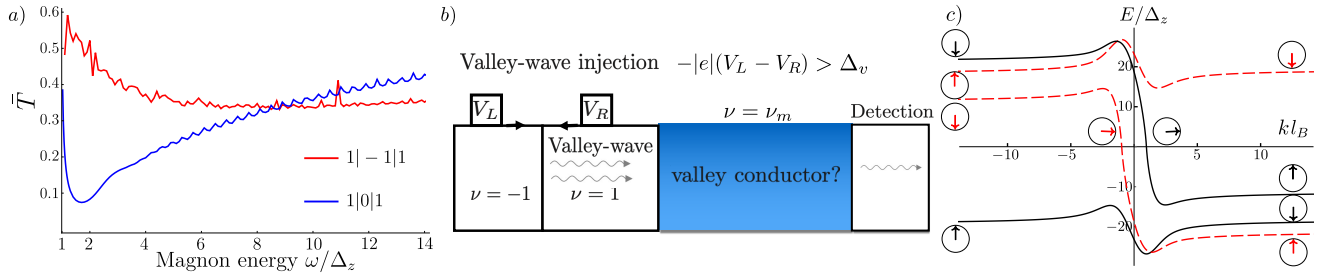


Figure 3. a) Angularly average magnon transmission $\bar{T}(\omega)$ v.s. ω . The parameters used in this calculation are the same as those in Fig. 2 b) Valley wave scattering devices. We propose to replace the $2|1$ junction used in Ref. [38, 39] with $-1|1$ junctions to generate valley waves. c) Bandstructure of a $-1|1$ junction used for valley-wave injection. All states color-coded with black and red are respectively fully polarized in K and K' valleys, while the spin rotates smoothly from \uparrow to \downarrow across the junction. The parameters for this calculation ($B = 8T$ and valley polarization energy $\Delta_v = 3.7\text{meV}$ correspond to the circumstances of Ref. [39]).

tum Hall ground-states, which remains an elusive target especially at fractional filling factors [35].

Acknowledgement:— We acknowledge helpful interactions with Hailong Fu, Andrea Young, Haoxin Zhou and Jun Zhu. This work is supported by DOE BES grant DE- FG02-02ER45958 and by Welch foundation grant TBF1473. N.W was partially supported by a Graduate School Continuing Fellowship.

-
- [1] N. Samarth, *Nature* **546**, 216 (2017).
 - [2] M. Gibertini, M. Koperski, A. Morpurgo, and K. Novoselov, *Nature nanotechnology* **14**, 408 (2019).
 - [3] K. S. Burch, D. Mandrus, and J.-G. Park, *Nature* **563**, 47 (2018).
 - [4] B. Huang, G. Clark, D. R. Klein, D. MacNeill, E. Navarro-Moratalla, K. L. Seyler, N. Wilson, M. A. McGuire, D. H. Cobden, D. Xiao, *et al.*, *Nature nanotechnology* **13**, 544 (2018).
 - [5] S. Jiang, L. Li, Z. Wang, K. F. Mak, and J. Shan, *Nature nanotechnology* **13**, 549 (2018).
 - [6] A. Chumak, V. Vasyuchka, A. Serga, and B. Hillebrands, *Nature Physics* **11**, 453 (2015).
 - [7] A. V. Chumak, arXiv preprint arXiv:1901.08934 (2019).
 - [8] S. M. Rezende, in *Fundamentals of Magnonics* (Springer, 2020) pp. 287–352.
 - [9] Y. Zhang, Z. Jiang, J. Small, M. Purewal, Y.-W. Tan, M. Fazlollahi, J. Chudow, J. Jaszczak, H. Stormer, and P. Kim, *Physical review letters* **96**, 136806 (2006).
 - [10] J. G. Checkelsky, L. Li, and N. P. Ong, *Phys. Rev. Lett.* **100**, 206801 (2008).
 - [11] X. Du, I. Skachko, F. Duerr, A. Luican, and E. Y. Andrei, *Nature* **462**, 192 (2009).
 - [12] A. F. Young, C. R. Dean, L. Wang, H. Ren, P. Cadden-Zimansky, K. Watanabe, T. Taniguchi, J. Hone, K. L. Shepard, and P. Kim, *Nature Physics* **8**, 550 (2012).
 - [13] A. Young, J. Sanchez-Yamagishi, B. Hunt, S. Choi, K. Watanabe, T. Taniguchi, R. Ashoori, and P. Jarillo-Herrero, *Nature* **505**, 528 (2014).
 - [14] M. O. Goerbig, *Rev. Mod. Phys.* **83**, 1193 (2011).
 - [15] M. O. Goerbig, R. Moessner, and B. Douçot, *Phys. Rev. B* **74**, 161407 (2006).
 - [16] J. Alicea and M. P. A. Fisher, *Phys. Rev. B* **74**, 075422 (2006).
 - [17] K. Yang, S. Das Sarma, and A. H. MacDonald, *Phys. Rev. B* **74**, 075423 (2006).
 - [18] R. L. Doretto and C. M. Smith, *Phys. Rev. B* **76**, 195431 (2007).
 - [19] I. F. Herbut, *Phys. Rev. B* **75**, 165411 (2007).
 - [20] J. Jung and A. H. MacDonald, *Phys. Rev. B* **80**, 235417 (2009).
 - [21] K. Nomura, S. Ryu, and D.-H. Lee, *Phys. Rev. Lett.* **103**, 216801 (2009).
 - [22] R. Nandkishore and L. Levitov, *Physica Scripta* **2012**, 014011 (2012).
 - [23] M. Kharitonov, *Phys. Rev. Lett.* **109**, 046803 (2012).
 - [24] M. Kharitonov, *Physical Review B* **85**, 155439 (2012).
 - [25] I. Sodemann and A. H. MacDonald, *Phys. Rev. Lett.* **112**, 126804 (2014).
 - [26] C. Dean, P. Kim, J. Li, and A. Young, *Fractional Quantum Hall Effects: New Developments*, 317 (2020).
 - [27] C. R. Dean, A. F. Young, I. Meric, C. Lee, L. Wang, S. Sorgenfrei, K. Watanabe, T. Taniguchi, P. Kim, K. L. Shepard, *et al.*, *Nature nanotechnology* **5**, 722 (2010).
 - [28] C. R. Dean, A. F. Young, P. Cadden-Zimansky, L. Wang, H. Ren, K. Watanabe, T. Taniguchi, P. Kim, J. Hone, and K. Shepard, *Nature Physics* **7**, 693 (2011).
 - [29] A. A. Zibrov, C. Kometter, H. Zhou, E. Spanton, T. Taniguchi, K. Watanabe, M. Zaletel, and A. Young, *Nature* **549**, 360 (2017).
 - [30] S. M. Girvin, in *Aspects topologiques de la physique en basse dimension. Topological aspects of low dimensional systems* (Springer, 1999) pp. 53–175.
 - [31] K. Nomura and A. H. MacDonald, *Phys. Rev. Lett.* **96**, 256602 (2006).
 - [32] D. A. Abanin, B. E. Feldman, A. Yacoby, and B. I. Halperin, *Phys. Rev. B* **88**, 115407 (2013).
 - [33] B. Hunt, J. Sanchez-Yamagishi, A. Young, M. Yankowitz, B. J. LeRoy, K. Watanabe, T. Taniguchi, P. Moon, M. Koshino, P. Jarillo-Herrero, *et al.*, *Science* **340**, 1427 (2013).
 - [34] F. Amet, J. Williams, K. Watanabe, T. Taniguchi, and D. Goldhaber-Gordon, *Physical review letters* **110**, 216601 (2013).
 - [35] A. Zibrov, E. Spanton, H. Zhou, C. Kometter, T. Taniguchi, K. Watanabe, and A. Young, *Nature*

- Physics **14**, 930 (2018).
- [36] L. Veyrat, C. Dép  rez, A. Coissard, X. Li, F. Gay, K. Watanabe, T. Taniguchi, Z. Han, B. A. Piot, H. Sellier, *et al.*, Science **367**, 781 (2020).
- [37] P. Stepanov, S. Che, D. Shcherbakov, J. Yang, R. Chen, K. Thilagar, G. Voigt, M. W. Bockrath, D. Smirnov, K. Watanabe, *et al.*, Nature Physics **14**, 907 (2018).
- [38] D. S. Wei, T. van der Sar, S. H. Lee, K. Watanabe, T. Taniguchi, B. I. Halperin, and A. Yacoby, Science **362**, 229 (2018).
- [39] H. Zhou, H. Polshyn, T. Taniguchi, K. Watanabe, and A. Young, Nature Physics, 1 (2019).
- [40] C. Huang, N. Wei, and A. MacDonald, in preparation.
- [41] G. Murthy, E. Shimshoni, and H. A. Fertig, Phys. Rev. B **93**, 045105 (2016).
- [42] J. R. M. de Nova and I. Zapata, Phys. Rev. B **95**, 165427 (2017).
- [43] F. Pientka, J. Waissman, P. Kim, and B. I. Halperin, Phys. Rev. Lett. **119**, 027601 (2017).
- [44] See Supplementary Material for the details of the model, the properties of the collective modes and the numeric methods to calculate transmission probability of collective modes.
- [45] N. Wei, C. Huang, and A. MacDonald, in preparation.
- [46] J. W. Negele, Rev. Mod. Phys. **54**, 913 (1982).
- [47] P. Ring and P. Schuck, *The nuclear many-body problem* (Springer Science & Business Media, 2004).
- [48] L. Gor'kov and I. Dzyaloshinskii, Sov. Phys. JETP **26**, 449 (1968).
- [49] C. Kallin and B. I. Halperin, Phys. Rev. B **30**, 5655 (1984).
- [50] J. Cao, H. A. Fertig, and L. Brey, "Quantum geometric exciton drift velocity," (2020), arXiv:2008.00259 [cond-mat.mes-hall].
- [51] P. Tikhonov, E. Shimshoni, H. Fertig, and G. Murthy, Physical Review B **93**, 115137 (2016).
- [52] J.-H. Zheng and M. A. Cazalilla, Phys. Rev. B **97**, 235402 (2018).
- [53] C. Huang and M. A. Cazalilla, Phys. Rev. B **92**, 155124 (2015).

Supplementary Materials

I. QUANTUM HALL MAGNETS: MEAN FIELD AND COLLECTIVE MODES

We give a systematic introduction to the collective modes in graphene quantum Hall magnet at integer filling fraction of the $N = 0$ Landau levels, *i.e.* $\nu = 0, 1$. Some of the results we discussed here can also be found in literature, see Ref. [S41–S43]. We first review the microscopic Hamiltonian projected onto $N = 0$ Landau level and its mean-field ground state at various filling fractions. Next, we study collective excitation of the mean-fields using time-dependent Hartree-Fock theory. This is a *conserving approximation* that conserve the symmetries of the microscopic Hamiltonian. Mathematically, we solve the so-called RPA equation whose roots describe the dispersion of collective modes. The results are summarized in Table. I and we neglect $\nu = \pm 2$ since they do not support intra-Landau level collective modes.

The microscopic Hamiltonian projected onto the $N = 0$ Landau-Level is given by the following:

$$\hat{\mathcal{H}} = \sum_k c_k^\dagger \hat{H}_k^0 c_k + \frac{1}{2} \sum_{\alpha=0}^3 \sum_{k,k',q_y} V_\alpha(k-k', q_y) : [c_{k+q_y}^\dagger \tau^\alpha c_k] [c_{k'}^\dagger \tau^\alpha c_{k'+q_y}] : . \quad (\text{S1})$$

The basis $c_k = (c_{kK\uparrow}, c_{kK\downarrow}, c_{kK'\uparrow}, c_{kK'\downarrow})^T$ has 4 components in valley (τ) and spin (s) space. The single-particle term is independent of k unless translation symmetry is broken (*e.g.* close to the edge or domain wall). We set the background potential $E_b(k) = 0$ in this section to discuss collective modes in the bulk, then \hat{H}_k^0 consists of the spin-splitting from the Zeeman effect (Δ_z) and a possible valley splitting from the sublattice polarization potential:

$$\hat{H}_k^0 = -\frac{\Delta_z}{2} s^z - \frac{\Delta_v}{2} \tau^z. \quad (\text{S2})$$

The second term in Eq. (S1) describes Coulomb interaction between particles in the $N = 0$ Landau level. The Coulomb scattering amplitude is given by the following:

$$V_\alpha(k-k', q_y) = \frac{1}{2\pi L_y} \int dq_x U_\alpha(\mathbf{q}) e^{-\mathbf{q}^2 l_B^2/2} e^{iq_x(k-k')l_B^2} \quad (\text{S3})$$

where we use $\alpha = 0, 1, 2, 3$ and $\alpha = 0, x, y, z$ interchangeably,

$$U_0(\mathbf{q}) = \frac{2\pi e^2}{\epsilon \sqrt{q^2 + \kappa^2}}, \quad U_i(\mathbf{q}) = 2\pi l_B^2 u_i, \quad i = x, y, z \quad (\text{S4})$$

Here U_0 is the long-range Coulomb potential and it has a infrared cut-off $\kappa \sim 1/L_y$ and we take the dielectric constant $\epsilon \approx 6.6$ from a Boron-Nitride substrate. Besides the long-range Coulomb interaction, the short-range valley anisotropic

interaction ($U_i(\mathbf{q})$) in graphene is also important in selecting the correct ground-states, as pointed out by Kharitonov [S23, S24]. This is because the short-range interaction reduce the $SU(4)$ symmetry of the U_0 Hamiltonian. Although momentum non-conserving (*i.e.* Umklapp) scattering process is allowed by the magnetic field, it is exponentially suppressed by a factor $e^{-(l_B/a)^2}$ where a is the lattice constant. So to a very good approximation, $u_x = u_y \equiv u_\perp$ and the resulting interacting Hamiltonian has an $U(1)_v$ symmetry. Furthermore, the experimental observation of metal-insulator phase transition of the edge states [S13, S24] have narrow down the relevant parameter space to

$$0 < -u_\perp < u_z \quad (\text{S5})$$

In all of our numeric calculations, we use valley anisotropic energies inferred from experiments[S13, S35]: $u_\perp = -4\Delta_z$ and $u_z = 7\Delta_z$ in the perpendicular magnetic field.

A. Mean-Field Ground State

We seek ground-state of Eq. (S1) with the following mean-field order parameter

$$P_{ki,k'j}^0 = \langle \Psi_{\text{QHM}} | c_{ki}^\dagger c_{k'j} | \Psi_{\text{QHM}} \rangle \quad (\text{S6})$$

Here Ψ_{QHM} is the Slater determinant ground-state to be determined self-consistently from variational principle. For translation invariant system, the order parameter can be block diagonalized into 4×4 momentum-independent matrices:

$$P_{ki,k'j}^0 = P_{ij}^0 \delta_{k,k'}. \quad (\text{S7})$$

As a result, the mean-field quasi-particle excitation is independent of k and the 4 energy levels are obtained by diagonalizing the following mean-field Hamiltonian:

$$\hat{h} = -\frac{\Delta_z}{2} s^z - \frac{\Delta_v}{2} \tau^z + \Sigma^H[\hat{P}] + \Sigma^F[\hat{P}], \quad (\text{S8a})$$

$$\Sigma^H[\hat{P}] = \sum_{i=x,y,z} u_i \text{tr}(\tau^i \hat{P}) \tau^i, \quad \Sigma^F[\hat{P}] = -u_0 \hat{P} - \sum_{i=x,y,z} \tau^i \hat{P} \tau^i \quad (\text{S8b})$$

where $u_0 = \int \frac{d\mathbf{q}}{(2\pi)^2} U_0(\mathbf{q}) e^{-\mathbf{q}^2 l_B^2/2}$ is the exchange energy. Note that in this subsection we focus on the ground state and therefore omit the superscript "0" for the simplicity of notation. The following two principles are useful guidelines to guess the correct ground state order parameter P_{ij} :

1. The exchange-energy of the dominant long-range Coulomb interaction (u_0) favors maximum isospin polarization, *i.e.* Quantum Hall ferromagnetsim.
2. If the short-range valley anisotropic interaction is a delta-function contact interaction $\delta(\mathbf{r}_i - \mathbf{r}_j)$, it does not scatter states with the same isospin due to Pauli exclusion principle.

$\nu = \pm 1$ – At filling factor $\nu = \pm 1$ one of the four bands is empty (fill). Due to principle 1, electrons (holes) will occupy the band with identical isospin polarization. Then, the “direction” of the isospin is solely selected by single-particle term and short-range Coulomb interactions does not play any role because of principle 2. Thus, the ground state of $\nu = \pm 1$ is spin and valley polarized with the order parameter

$$P_{\nu=-1} = |K \uparrow\rangle \langle K \uparrow|, \quad P_{\nu=1} = \mathbf{1} - |K' \downarrow\rangle \langle K' \downarrow| \quad (\text{S9})$$

Energy levels of quasiparticle excitation are shown in Fig. S1. Bearing in mind the energy scale Eq. (S5) and experimental observation $-2u_\perp > \Delta_z$ in perpendicular magnetic field, we can understand the excited state ordering as follow. The three excited states are all separated from the ground-state by u_0 due to reversal of isospin. For a sample without sublattice polarization $\Delta_v = 0$, excited states that flip valley polarization will require less energy because of Eq. (S5). When $-2u_\perp > \Delta_z$, the first excited state flips both spin and valley while the second excited state only flips valley. This band ordering excitation can be experimentally adjust by a sublattice polarization potential Δ_v and in-plane magnetic field. Due to particle-hole symmetry, we obtain the band ordering of $\nu = 1$ state by flipping the band ordering of $\nu = -1$ state and interchanging the isospin $K \leftrightarrow K'$ and $\uparrow \leftrightarrow \downarrow$ [S32]. Before moving to the $\nu = 0$

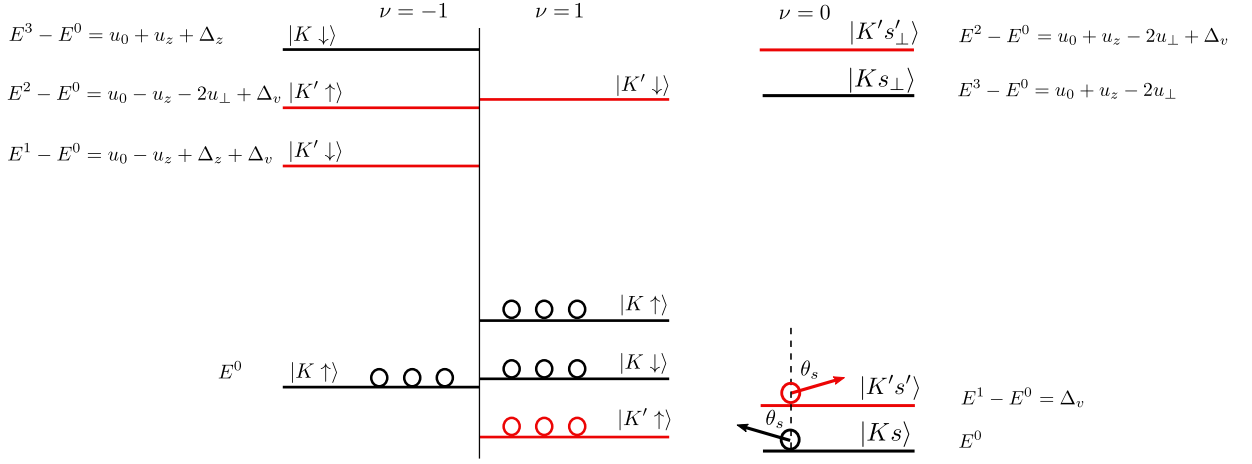


Figure S1. A schematic of the energy levels and eigenstates of $\nu = \pm 1$ and $\nu = 0$ QHMs. The expression of E^n measured from the lowest level are provided for $\nu = -1, 0$ QHMs, while the level spacing in $\nu = 1$ QHM can be derived from $\nu = -1$ by a particle-hole transformation. Both of $\nu = \pm 1$ QHMs are assumed to be fully valley-polarized by a weak valley polarization energy Δ_v . For $\nu = 0$, Δ_v splits the otherwise degenerate (un)occupied bands. The arrows in the occupied bands represent the spin orientation with canting angle θ_s .

case, let us mention that when $\Delta_v = 0$ the ground state at $\nu = \pm 1$ is subtle because the many-body Hamiltonian projected into the subspace of the valley-polarized states have a valley SU(2) symmetry, indicating that the system has to spontaneously choose a valley polarization. Finite temperature and disorder effect [S32] will play an important role in this case. Note however, when $\nu = \pm 1$ state forms a junction the valley degeneracy will be lifted [S45] and we can safely assume the ground state at $\nu = \pm 1$ is polarized in K or K' valley.

$\nu = 0$ – The charge neutral ($\nu = 0$) state has to fill two out of the four $N = 0$ Landau levels. Because the two occupied states have to be orthogonal to each other principle 1 does not select the ground state. If there were no single particle terms, the two occupied states will be polarized in opposite valley to minimize the u_z self energy, and the spin in the two valley will polarize in opposite direction to minimize the $-u_\perp > 0$ self-energy.

Since valley and sublattice are locked in $N = 0$ Landau level, this means the ground state is an antiferromagnet. In the presence of finite Zeeman term, spins in opposite valley will cant towards the direction of total magnetic field and the ground state becomes a canted antiferromagnet (CAF), see Ref. [S24] for more discussion. The order parameter of CAF is given by $P_{\nu=0} = 1/2 + \cos \theta_s s^z / 2 + \sin \theta_s \tau^z (\cos \phi s^x + \sin \phi s^y) / 2$ where θ_s is the canting angle satisfying $\cos \theta_s = \Delta_z / 4|u_\perp|$. Due to the $U(1)$ symmetry of the spin rotation about z axis, we take $\phi = 0$. Physically, it means that the Néel vector of CAF state $\mathbf{l} = \text{tr}(\tau^z \mathbf{s} P) / 2$ spontaneously polarizes in the x direction.

The energy levels and excitation spectrum of $\nu = 0$ is shown in Fig. 1b. The four eigenvectors are z^n :

$$z^0 = |Ks\rangle, \quad z^1 = |K's'\rangle, \quad z^2 = |K's'_\perp\rangle, \quad z^3 = |Ks_\perp\rangle. \quad (\text{S10})$$

where $|s\rangle / |s'\rangle = (\cos \frac{\theta_s}{2}, \pm \sin \frac{\theta_s}{2})^T$ and $|s_\perp\rangle / |s'_\perp\rangle = (\sin \frac{\theta_s}{2}, \mp \cos \frac{\theta_s}{2})^T$. Due to spin-canting, the excited state energy is independent of Zeeman energy.

B. The RPA kernel and the normal modes of Quantum Hall Magnets

The excitations for both $\nu = 0$ and $\nu = \pm 1$ we discussed so far are quasiparticle charge excitation. In this section, we discuss neutral collective excitation that typically occurs at much smaller energy scale. In the main text, we have already sketched the derivation of the RPA equation. The expression of RPA kernel reads

$$\mathbb{K}_{kmn}^{k'm'n'}(q_y) = (E_{k+q_y}^m - E_k^n) \delta_{kk'} \delta_{mm'} \delta_{nn'} + (f_{n,k} - f_{m,k}) \left(\tilde{V}_{mnn'm'}(k, k', q_y) - \tilde{V}_{mm'n'n}(k' + q_y, k', k - k') \right), \quad (\text{S11})$$

$$\tilde{V}_{mnn'm'}(k, k', q_y) = \sum_{\alpha} V_{\alpha}(k - k', q_y) z_k^{m\dagger} \tau^{\alpha} z_{k+q_y}^n z_{k'+q_y}^{n'\dagger} \tau^{\alpha} z_{k'}^{m'} \quad (\text{S12})$$

In homogeneous QHMs, the quasiparticle spinors $z_k^m \equiv z^m$, energy $E_k^m \equiv E^m$ and the Fermi-Dirac distribution $f_{m,k} \equiv f_m$ are independent of the momentum k . Due to translation invariance, the RPA kernel $\mathbb{K}_{kmn}^{k'm'n'}(q_y)$ is a

function of $\Delta k = k' - k$ so it can be block diagonalized by Fourier transformation:

$$\begin{aligned} & \mathbb{K}_{mn}^{m'n'}(\mathbf{q}) \\ &= \frac{1}{L_y} \sum_{\Delta k} \mathbb{K}_{k-\frac{\Delta k}{2}mn}^{k+\frac{\Delta k}{2}m'n'}(q_y) e^{-iq_x \Delta k l_B^2} \\ &= (E^m - E^n) \delta_{mm'} \delta_{nn'} + (f_n - f_m) \left[\sum_{i=x,y,z} u_i(\mathbf{q}) z^{m\dagger} \tau^\alpha z^n z^{n'\dagger} \tau^\alpha z^{m'} - \sum_{\alpha=0,x,y,z} u_\alpha(\mathbf{q}) z^{m\dagger} \tau^\alpha z^{m'} z^{n'\dagger} \tau^\alpha z^n \right], \end{aligned} \quad (\text{S13})$$

where $u_\alpha(\mathbf{q}) = \int \frac{d\mathbf{k}}{(2\pi)^2} U_\alpha(\mathbf{k}) e^{-\mathbf{k}^2 l_B^2/2} e^{-i\mathbf{q} \cdot \mathbf{k} l_B^2}$ only depends on the magnitude of the wave vector \mathbf{q} . In particular, $u_i(\mathbf{q}) = u_i e^{-\mathbf{q}^2 l_B^2/2}$ and in the $\kappa = 0$ limit $u_0(\mathbf{q}) = u_0 e^{-\mathbf{q}^2 l_B^2/4} I_0(\mathbf{q}^2 l_B^2/4)$ where $u_0 = \sqrt{\pi/2} e^2 / \epsilon l_B$ and $I_0(x)$ is the modified Bessel function of the first kind. The particle-hole pairs (mn) 's fulfill $f_m \neq f_n$. Therefore, the isotropic ($\alpha = 0$) Hartree term does not appear in the first summation in the last line since $z^{m\dagger} z^n = 0$. As a result, the RPA equation in the main text can be simplified as

$$\omega(\mathbf{q}) \phi_{mn}(\mathbf{q}) = \sum_{m'n'} \mathbb{K}_{mn}^{m'n'}(\mathbf{q}) \phi_{m'n'}(\mathbf{q}), \quad (\text{S14})$$

where by definition

$$\phi_{mn}(\mathbf{q}) = \frac{1}{L_y} \sum_k \psi_{k-\frac{q_y}{2}mn}(q_y, \omega(\mathbf{q})) e^{-iq_x k l_B^2} \quad (\text{S15})$$

represents a normal mode of the density matrix fluctuation. One can explicitly verify that $\tilde{\phi}_{mn} = \phi_{nm}^*(-\mathbf{q})$ is another normal mode with frequency $-\omega(\mathbf{q})$ from Eq. (S14) and $\mathbb{K}_{mn}^{m'n'} = -(\mathbb{K}_{nm}^{n'm'})^*$. Both modes must coexist in the system to preserve the hermiticity of the density matrix $\hat{P}(t)$. To avoid the redundancy, we only focus on the positive-frequency modes in the following.

$\nu = 0$ *collective modes*– The $\nu = 0$ state has *eight* particle-hole(p-h) transitions ϕ_{mn} which we labelled by $(mn) = (30), (21), (03), (12), (20), (02), (31), (13)$. The index m (n) represents the unoccupied (occupied) band. From Fig. 1b), we see that the first four pairs are intravalley excitations, while the last four are intervalley excitations. Using them as a basis to construct the matrix $\hat{\mathbb{K}}(\mathbf{q})$ in Eq. (S13), we found it can be block diagonalized into two 4×4 matrices,

$$\hat{\mathbb{K}}(\mathbf{q}) = \begin{pmatrix} \hat{\mathbb{K}}^{\text{intra}}(\mathbf{q}) & 0 \\ 0 & \hat{\mathbb{K}}^{\text{inter}}(\mathbf{q}) \end{pmatrix}. \quad (\text{S16})$$

where the RPA kernel in intravalley and intervalley subspace is given by the following:

$$\hat{\mathbb{K}}^{\text{inter}}(\mathbf{q}) = \begin{pmatrix} \hat{\mathbb{K}}^3(\mathbf{q}) & 0 \\ 0 & \hat{\mathbb{K}}^4(\mathbf{q}) \end{pmatrix}, \quad (\text{S17a})$$

$$\hat{\mathbb{K}}^{3,4}(\mathbf{q}) = \begin{pmatrix} \Delta_g - u_0(\mathbf{q}) + u_z(\mathbf{q}) + 2u_\perp(\mathbf{q}) \sin^2 \theta_s \pm \Delta_v & 2u_\perp(\mathbf{q}) \sin^2 \theta_s \\ -2u_\perp(\mathbf{q}) \sin^2 \theta_s & -(\Delta_g - u_0(\mathbf{q}) + u_z(\mathbf{q}) + 2u_\perp(\mathbf{q}) \sin^2 \theta_s \pm \Delta_v) \end{pmatrix}. \quad (\text{S17b})$$

$$\hat{\mathbb{K}}^{\text{intra}}(\mathbf{q}) = \begin{pmatrix} \Delta_g - u_0(\mathbf{q}) - u_z(\mathbf{q}) & 2u_\perp(\mathbf{q}) \cos^2 \theta_s & -2u_\perp(\mathbf{q}) \sin^2 \theta_s & 0 \\ 2u_\perp(\mathbf{q}) \cos^2 \theta_s & \Delta_g - u_0(\mathbf{q}) - u_z(\mathbf{q}) & 0 & -2u_\perp(\mathbf{q}) \sin^2 \theta_s \\ 2u_\perp(\mathbf{q}) \sin^2 \theta_s & 0 & -(\Delta_g - u_0(\mathbf{q}) - u_z(\mathbf{q})) & -2u_\perp(\mathbf{q}) \cos^2 \theta_s \\ 0 & 2u_\perp(\mathbf{q}) \sin^2 \theta_s & -2u_\perp(\mathbf{q}) \cos^2 \theta_s & -(\Delta_g - u_0(\mathbf{q}) - u_z(\mathbf{q})) \end{pmatrix}, \quad (\text{S18})$$

where $\Delta_g = u_0 + u_z - 2u_\perp$ is the bulk gap of CAF state without any sublattice polarization potential, $\Delta_v = 0$.

The eigenvalues of $\hat{\mathbb{K}}^{\text{inter}}$ and $\hat{\mathbb{K}}^{\text{intra}}$ are the intervalley and intravalley collective mode dispersion. Their dispersion is documented in Table. I. We found the intervalley modes have large excitation gaps $\omega_{3,4}(\mathbf{q} = 0) \sim 11\Delta_z \mp \Delta_v$ so they do not contribute to nonlocal spin-transport experiments which typically occurs at energy scale $\lesssim 5\Delta_z$. In contrast, intravalley modes, namely the (gapless) Néel mode ϕ^1 and the Larmor mode ϕ^2 play a significant role in nonlocal

spin transport experiments. In the basis $\{(30), (21), (03), (12)\}$, their wave functions are given by the following in

$$\phi^\alpha(\mathbf{q}) = (u_{\mathbf{q}}^\alpha, (-1)^{\alpha-1}u_{\mathbf{q}}^\alpha, v_{\mathbf{q}}^\alpha, (-1)^{\alpha-1}v_{\mathbf{q}}^\alpha)^T \quad (\text{S19a})$$

$$u_{\mathbf{q}}^\alpha = \frac{1}{2}\sqrt{1 + \frac{\xi_\alpha(\mathbf{q})}{\omega_\alpha(\mathbf{q})}}, \quad v_{\mathbf{q}}^\alpha = \frac{1}{2}\sqrt{-1 + \frac{\xi_\alpha(\mathbf{q})}{\omega_\alpha(\mathbf{q})}}, \quad (\text{S19b})$$

$$\xi_\alpha(\mathbf{q}) = \Delta_g - u_0(\mathbf{q}) + u_z(\mathbf{q}) + (-1)^\alpha u_\perp(\mathbf{q}) \cos^2 \theta_s, \quad \alpha = 1, 2. \quad (\text{S19c})$$

It is easy to verify that $(u_{\mathbf{q}}^\alpha)^2 - (v_{\mathbf{q}}^\alpha)^2 = 1/2$ and hence the wave functions satisfy the normalization condition

$$\sum_{mn} (f_m - f_n) \bar{\phi}_{mn}^\alpha(\mathbf{q}) \phi_{mn}^\beta(\mathbf{q}) = \delta^{\alpha\beta}. \quad (\text{S20})$$

where $\bar{\phi}$ is the complex conjugate of ϕ . We note the Kernel matrix $\hat{\mathbb{K}}^{\text{intra}}(\mathbf{q})$ has an addition \mathbb{Z}_2 symmetry $\mathbf{1} \otimes \rho^x$ such that $[\mathbf{1} \otimes \rho^x, \hat{\mathbb{K}}^{\text{intra}}(\mathbf{q})] = 0$, where ρ^x is the 1st Pauli matrix. One can easily check $\mathbf{1} \otimes \rho^x \phi^{1,2}(\mathbf{q}) = \pm \phi^{1,2}(\mathbf{q})$. Therefore, the gapless Néel mode and the Larmor mode with Zeeman gap are respectively the symmetric and anti-symmetric combinations of the spin-flipping excitation in two valleys (or sublattice).

In order to understand dynamics of the observables, we first use the excited state wavefunctions of the RPA equation to construct the fluctuating density matrix:

$$\begin{aligned} \rho_{ij}(\mathbf{r}, t) &= \langle \Psi_{\text{QHM}}(t) | \hat{\psi}_j^\dagger(\mathbf{r}) \hat{\psi}_i(\mathbf{r}) | \Psi_{\text{QHM}}(t) \rangle \\ &= \frac{1}{L_y} \sum_{k, q_y} \frac{1}{\sqrt{\pi} l_B} e^{-\frac{(x - k l_B^2)^2}{l_B^2} - \frac{q_y^2 l_B^2}{4}} e^{i q_y y} P_{k + \frac{q_y}{2} i, k - \frac{q_y}{2} j}(t) \\ &= P_{ij}^0 + \sum_{l=1,2} \int \left[\delta P_{ij}^l(\mathbf{q}) e^{i(\mathbf{q} \cdot \mathbf{r} - \omega_l(\mathbf{q})t)} + (\delta P_{ji}^l(\mathbf{q}))^* e^{-i(\mathbf{q} \cdot \mathbf{r} - \omega_l(\mathbf{q})t)} \right] \frac{d\mathbf{q}}{(2\pi)^2} \end{aligned} \quad (\text{S21})$$

where we have expanded the density matrix to linear order in deviation

$$P_{k + \frac{q_y}{2} i, k - \frac{q_y}{2} j}(t) = \langle \Psi_{\text{QHM}}(t) | c_{k - \frac{q_y}{2} j}^\dagger c_{k + \frac{q_y}{2} i} | \Psi_{\text{QHM}}(t) \rangle = P_{ij}^0 \delta_{q_y, 0} + \delta P_{k + \frac{q_y}{2} i, k - \frac{q_y}{2} j}(t) + O(\delta P^2) \quad (\text{S22})$$

here P_{ij}^0 is the ground state order parameter discussed in Sec. I A. The integral in the last line of Eq. (S21) is obtained by expanding $\delta \hat{P}(t)$ in terms of normal modes. The first and second integrands correspond to positive- and negative-frequency modes, respectively. Comparing with the definition of the normal mode wave function, Eq. (S15), we arrive at the following relation,

$$\delta P_{ij}^l(\mathbf{q}) = a^l(\mathbf{q}) \sum_{mn} \phi_{mn}^l(\mathbf{q}) z_i^m z_j^{n\dagger} \quad (\text{S23})$$

where the small parameter a^l denotes the amplitude of the l th normal mode. Substituting the $\nu = 0$ quasiparticle spinors Eq. (S10) into the above equation and using the long-wavelength limit of the dispersion,

$$\omega_1(\mathbf{q}) \approx v_{\text{AF}} |\mathbf{q}|, \quad v_{\text{AF}} l_B^{-1} = \sqrt{[u_0 + 2u_z + 4|u_\perp|] |u_\perp| \sin^2 \theta_s}, \quad (\text{S24})$$

we arrive at the following:

$$\delta \hat{P}^1(\mathbf{q}) / a^1(\mathbf{q}) = i \tau^z s^y + \frac{v_{\text{AF}} |\mathbf{q}|}{4|u_\perp| \sin^2 \theta_s} (\sin \theta_s s^z - \cos \theta_s \tau^z s^x + i \tau^z s^y) + O(q^2 l_B^2), \quad (\text{S25a})$$

$$\delta \hat{P}^2(\mathbf{q}) / a^2(\mathbf{q}) = -\cos \theta_s (s^x - i s^y) + \sin \theta_s \tau^z s^z + O(q^2 l_B^2). \quad (\text{S25b})$$

At $\mathbf{q} = 0$, ϕ^1 or Eq. (S25a) describes a global rotation of Néel vector which costs zero energy, see Table. I. It disperses linearly at finite q and in addition to the fluctuation of azimuthal angle of the Néel vector, it also generates fluctuation of spin-density along the broken symmetry direction, i.e. z . In Eq. (S25b), the first term describes

Table I. A list of collective mode dispersion of $\nu = 0$ CAF phase and $\nu = 1$ valley-and-spin-polarized QHM.

ν	collective mode	dispersion
0	gapless mode ϕ^1 /Larmor mode ϕ^2	$\omega_{1,2} = \sqrt{[\Delta_g - u_0(\mathbf{q}) - u_z(\mathbf{q}) \pm 2u_\perp(\mathbf{q}) \cos^2 \theta_s]^2 - 4u_\perp^2(\mathbf{q}) \sin^4 \theta_s}$
	intervalley mode $\phi^{3,4}$	$\omega_{3,4} = \sqrt{(\Delta_g - u_0(\mathbf{q}) + u_z(\mathbf{q}))(\Delta_g - u_0(\mathbf{q}) + u_z(\mathbf{q}) + 4u_\perp(\mathbf{q}) \sin^2 \theta_s) \mp \Delta_v}$
1	spin wavey(magnon) ϕ^1	$\omega_s = u_0 - u_0(\mathbf{q}) + u_z - u_z(\mathbf{q}) + \Delta_z$
	valley wave ϕ^2	$\omega_v = u_0 - u_0(\mathbf{q}) - (u_z - u_z(\mathbf{q})) - 2(u_\perp - u_\perp(\mathbf{q})) + \Delta_v$
	spin-valley wave ϕ^3	$\omega_{vs} = u_0 - u_0(\mathbf{q}) - (u_z - u_z(\mathbf{q})) + \Delta_z + \Delta_v$

precession of total spin about the z axis ($s^x - is^y = s^-$ is a spin-lowering operator) so this corresponds to the Larmor mode that has an energy gap of Zeeman energy, see Table. 1. Because the Néel vector has to be perpendicular to total spin-polarization locally ($\mathbf{s} \cdot \mathbf{l} = 0$), the Larmor mode will also tilt the Néel vector towards to z direction and this is describes by the second term in Eq. (S25b).

$\nu = 1$ *collective modes*– Let us label the particle-hole excitation of $\nu = 1$ mode by the compound index $(mn) = (10), (20), (30), (01), (02), (03)$. They constitute a basis under which the 6×6 matrix $\mathbb{K}(\mathbf{q})$ is diagonal. The first three excitations have positive frequencies and are listed in Table. I. The corresponding normal modes are

$$\phi^1 = (1, 0, 0, \dots)^T, \quad \phi^2 = (0, 1, 0, \dots)^T, \quad \phi^3 = (0, 0, 1, 0, \dots)^T. \quad (\text{S26})$$

$\nu = -1$ QHM has the same collective mode dispersion due to the particle-hole symmetry. Among all these collective modes, we mainly focus on the magnons in the main text. From Table. I, we derive the long-wave length approximation of the magnon dispersions,

$$\omega_s(\mathbf{q}) = \Delta_z + 2\rho_s \mathbf{q}^2, \quad \rho_s l_B^{-2} = \frac{u_0}{8} + \frac{u_z}{4}. \quad (\text{S27})$$

When $\frac{\Delta_z}{4|u_\perp|} \ll 1$, the $\nu = \pm 1$ magnons have lower energy than $\nu = 0$ magnon, $\omega = \omega_s(\mathbf{q}) < \omega_1(\mathbf{q})$, except for $\omega < \Delta_z(1 + 2\rho_s \Delta_z / v_{\text{AF}}^2)$, which is however merely a narrow range because

$$\frac{2\rho_s \Delta_z}{v_{\text{AF}}^2} = \frac{(\frac{u_0}{4} + \frac{u_z}{2})\Delta_z}{(u_0 + 2u_z + 4|u_\perp|)|u_\perp|} < \frac{\Delta_z}{4|u_\perp|}. \quad (\text{S28})$$

Note that we used $\sin \theta_s \approx 1$ to simplify the analysis.

II. NUMERICAL METHOD TO CALCULATE THE S-MATRIX OF COLLECTIVE MODES IN QUANTUM HALL MAGNET (QHM) JUNCTIONS

In this section, we describe a numerical method to calculate the transmission probability of collective modes from the RPA equation. For simplicity, we focus on a one-dimensional scattering problem defined in the x direction and apply periodic boundary condition in the y -direction. In the Landau gauge, the momentum k describing the plane-wave along the y -direction also means the wavefunction is localized at the guiding center coordinate $X = kl_B^2$. The guiding centers are equally spaced $X_i - X_{i-1} = 2\pi/L_y$ in a system with fixed width L_y . Let the scattering geometry (i.e. QHM junction) be described by a set of guiding centers $\{X_i | i = 1, \dots, N\}$ and we study the transmission probability of an incoming collective mode in $X < X_1$ to an outgoing collective mode in $X > X_N$. Recall in the maintext, we use a compact notation $\psi_{kmn}(q_y, \omega)$ to describe particle-hole transition between band m and n with transverse momentum q_y and frequency ω . The collective modes of the homogeneous QHM are the asymptotic states of the scattering problem.

From here and what follows, we use $k = Xl_B^2$ interchangeably and the superscripts α, β and (α', β') to label collective modes in $X < X_1$ and $X > X_N$ region. They are given by the following:

$$\psi_{Xmn}(q_y, \omega) = \begin{cases} \frac{1}{\sqrt{v_\alpha}} \phi_{mn}^\alpha(q_x^\alpha, q_y) e^{iq_x^\alpha X} + \sum_\beta r_{\beta\alpha} \frac{1}{\sqrt{v_\beta}} \phi_{mn}^\beta(-q_x^\beta, q_y) e^{-iq_x^\beta X}, & X \leq X_1 \\ \sum_{\beta'} t_{\beta'\alpha} \frac{1}{\sqrt{v_{\beta'}}} \phi_{mn}^{\beta'}(q_x^{\beta'}, q_y) e^{iq_x^{\beta'} X}, & X \geq X_N \end{cases} \quad (\text{S29})$$

where the normal component of the wave vector q_x^α is a positive solution to the following equation,

$$\omega_\alpha(q_x^\alpha, q_y) = \omega, \quad (\text{S30})$$

and $v_\alpha = (dq_x^\alpha/d\omega)^{-1}$ is the velocity of the collective mode.

The unknown parameters r and t in Eq. (S29) can be eliminated using the normalization condition Eq. (S20) and the wavefunction at the start of the junction $X = X_1$ and end of the junction $X = X_N$:

$$r_{\beta\alpha} = \left[-\delta_{\alpha\beta} e^{iq_x^\alpha X_1} + \sqrt{v_\beta} \sum_{mn} (f_n - f_m) \bar{\phi}_{mn}^\beta(-q_x^\beta, q_y) \psi_{X_1 mn} \right] e^{iq_x^\beta X_1}, \quad (\text{S31a})$$

$$t_{\beta'\alpha} = \sqrt{v_{\beta'}} \sum_{mn} (f_n - f_m) \bar{\phi}_{mn}^{\beta'}(q_x^{\beta'}, q_y) \psi_{X_N mn} e^{-iq_x^{\beta'} X_N}. \quad (\text{S31b})$$

Next, we substitute Eq. (S31) and Eq. (S29) into the RPA equation in the main text, we arrive at the main equation to be solved numerically:

$$\sum_{i'=1}^N \sum_{m'n'} \left[(\mathbb{K}^{\text{eff}})_{X_i mn}^{X_i' m' n'}(q_y, \omega) - \omega \delta_{ii'} \delta_{mm'} \delta_{nn'} \right] \psi_{X_i' m' n'}(q_y, \omega) = V_{X_i mn}^\alpha(q_y, \omega), \quad 1 \leq i \leq N \quad (\text{S32})$$

Eq. (S32) is the RPA equation of maintext (Eq. 5) expressed in a finite domain where states to the left $X \leq X_1$ and to the right $X \geq X_N$ are fixed. The effective RPA Kernel \mathbb{K}^{eff} accounts for the (super) self-energy from states in $X < X_1$ and $X > X_N$:

$$\hat{\mathbb{K}}^{\text{eff}}(q_y, \omega) = \hat{\mathbb{K}}(q_y) + \hat{\Sigma}^L(q_y, \omega) + \hat{\Sigma}^R(q_y, \omega), \quad (\text{S33a})$$

$$(\Sigma^L)_{Xmn}^{X' m' n'}(q_y, \omega) = \delta_{X', X_1} (f_n - f_m) \sum_{\beta} \sum_{j < 1} \sum_{\bar{m}\bar{n}} \mathbb{K}_{Xmn}^{X_j \bar{m}\bar{n}}(q_y) e^{-iq_x^\beta (X_j - X_1)} \phi_{\bar{m}\bar{n}}^\beta(-q_x^\beta, q_y) \bar{\phi}_{mn}^\beta(-q_x^\beta, q_y), \quad (\text{S33b})$$

$$(\Sigma^R)_{Xmn}^{X' m' n'}(q_y, \omega) = \delta_{X', X_N} (f_n - f_m) \sum_{\beta'} \sum_{j > N} \sum_{\bar{m}\bar{n}} \mathbb{K}_{Xmn}^{X_j \bar{m}\bar{n}}(q_y) e^{iq_x^{\beta'} (X_j - X_N)} \phi_{\bar{m}\bar{n}}^{\beta'}(q_x^{\beta'}, q_y) \bar{\phi}_{mn}^{\beta'}(q_x^{\beta'}, q_y); \quad (\text{S33c})$$

In addition to the renormalization of RPA kernel, the incoming wave also introduces a source term in the RHS of Eq. (S32):

$$V_{Xmn}^\alpha(q_y, \omega) = \delta_{X, X_1} \frac{1}{\sqrt{v_\alpha}} \phi_{mn}^\alpha(-q_x^\alpha, q_y) \sum_{i' < 1} e^{-iq_x^\alpha (X_{i'} - X_1)} - e^{iq_x^\alpha X_{i'}}. \quad (\text{S34})$$

Note that for given (q_y, ω) , $(\mathbb{K}^{\text{eff}})_{Xmn}^{X' m' n'}$ and V_{Xmn}^α are fully determined without any unknown parameters, so the linear equation Eq. (S32) can be solved straightforwardly. From the output wave function ψ_{Xmn} , we can read out $r_{\alpha\beta}$ and $t_{\alpha\beta'}$ from Eqs. (S31).

Similarly, if a collective mode $\phi^{\alpha'}(\mathbf{q})$ is injected from the right, the asymptotic wave function reads that

$$\psi_{Xmn}(q_y, \omega) = \begin{cases} \sum_{\beta} t'_{\beta\alpha'} \frac{1}{\sqrt{v_\beta}} \phi_{mn}^\beta(q_x^\beta, q_y) e^{-iq_x^\beta X}, & X \leq X_1 \\ \frac{1}{\sqrt{v_{\alpha'}}} \phi_{mn}^{\alpha'}(q_x^{\alpha'}, q_y) e^{-iq_x^{\alpha'} X} + \sum_{\beta'} r'_{\beta'\alpha'} \frac{1}{\sqrt{v_{\beta'}}} \phi_{mn}^{\beta'}(q_x^{\beta'}, q_y) e^{iq_x^{\beta'} X}, & X \geq X_N \end{cases} \quad (\text{S35})$$

Following a similar procedure, we can evaluate $r'_{\alpha\beta}$ and $t'_{\alpha\beta'}$. The S-matrix of the QHM junction is constructed as follows:

$$S(q_y, \omega) = \begin{pmatrix} r_{\beta\alpha} & t'_{\beta\alpha'} \\ t_{\beta'\alpha} & r'_{\beta'\alpha'} \end{pmatrix}. \quad (\text{S36})$$

In the main text, we studied the magnon scattering problem in $\nu = 1|\nu_m|1$ QHM junctions. Because the microscopic Hamiltonian, Eq. (S1), conserves the total valley quantum number and the mean-field quasiparticle states do not mix different valleys (see Fig.1 in the maintext and Ref. [S45]), the magnon, as an intravalley mode, is decoupled from intervalley excitations. Consequently, the S-matrix of the magnon at a given parallel momentum q_y and energy ω is

$$\text{reduced to a } 2 \times 2 \text{ matrix, } \begin{pmatrix} r(q_y, \omega) & t(q_y, \omega) \\ t(q_y, \omega) & r'(q_y, \omega) \end{pmatrix}.$$